







RESEARCH ARTICLE | AUGUST 01 2023

Application of a hyperspectral camera for *in situ* plasma–material interaction studies at the linear plasma device PSI-2

Changjun Li ; Sebastijan Brezinsek  ; Stephan Ertmer; Arkadi Kreter ; Michael Reinhart; Rui Ding  ; Junling Chen



Rev. Sci. Instrum. 94, 083501 (2023)

<https://doi.org/10.1063/5.0155722>




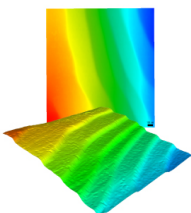
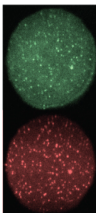


View
Online



Export
Citation

CrossMark

 MCL MAD CITY LABS INC. www.madcylabs.com	<p>Nanopositioning Systems</p> 	<p>Modular Motion Control</p> 	<p>AFM and NSOM Instruments</p> 	<p>Single Molecule Microscopes</p> 
---	--	--	---	--

Application of a hyperspectral camera for *in situ* plasma-material interaction studies at the linear plasma device PSI-2

Cite as: Rev. Sci. Instrum. 94, 083501 (2023); doi: 10.1063/5.0155722

Submitted: 23 April 2023 • Accepted: 12 July 2023 •

Published Online: 1 August 2023



Changjun Li,^{1,2} Sebastijan Brezinsek,^{2,3,a)} Stephan Ertmer,² Arkadi Kreter,² Michael Reinhart,² Rui Ding,^{1,a)} and Junling Chen¹

AFFILIATIONS

¹ Institute of Plasma Physics, Chinese Academy of Sciences, Hefei 230031, People's Republic of China

² Forschungszentrum Jülich GmbH-Institut für Energie- und Klimaforschung-Plasmaphysik, Partner of the Trilateral Euregio Cluster (TEC), 52425 Jülich, Germany

³ Institut für Laser- und Plasmaphysik, Heinrich-Heine-Universität Düsseldorf, 40225 Düsseldorf, Germany

^{a)} Authors to whom correspondence should be addressed: s.brezinsek@fz-juelich.de and rding@ipp.ac.cn

ABSTRACT

A hyperspectral camera (HSC-type Specim IQ) has been applied at the linear plasma device PSI-2 under steady-state conditions. The camera has the capacity of hyperspectral imaging (HSI) with the dimension of a data array $512 \times 512 \times 204$ (x, y, λ) covering the spectral span from 400 to 1000 nm with moderate average spectral resolution (FWHM ~ 7 nm). After radiometric calibration and background/continuum emission subtraction, two main applications of the camera, (i) plasma diagnostics in helium (He) plasmas and (ii) plasma-material interaction studies with tungsten (W) targets in neon (Ne) plasmas, have been carried out. The measurements were complemented by a movable Langmuir double probe system (LP) measuring electron temperature (T_e) and electron density (n_e) in radial direction r and a fiber-coupled cross-dispersion spectrometer with high spectral resolution (Spectrelle) recording neutral He, W, and Ne emission lines over the full plasma column. (i) Two-dimensional (2D) imaging of T_e and n_e radial profiles in axial direction z of the He plasma column were for the first time obtained by the regression analysis of T_e and n_e (from LP) and six He I line ratios (from HSC). The spatially resolved plasma parameters covered in these studies range between $T_e \sim 0.8\text{--}13.4$ eV and $n_e \sim 0.2 \times 10^{18}\text{--}3.9 \times 10^{18} \text{ m}^{-3}$ and permit a reconstruction of the plasma conditions in PSI-2 in 2D without LP perturbation. (ii) W sputtering was studied *in situ* in Ne plasmas exposing W target samples (negatively biased at 100 V) under perpendicular Ne plasma impact. Simultaneously, the 2D distributions of W (W I line at 429.5 nm) in front of the target and the 2D Ne plasma distribution (Ne I line at 703.2 nm) were recorded with complete spectral separation as confirmed by the Spectrelle spectrometer. This permits the simultaneous measurement of the neutral W penetration and its angular distribution induced in the sputtering process and of the impinging plasma distribution. The HSI technique offers, despite a few technical drawbacks, such as the moderate spectral resolution and poor time resolution, a new possibility to distinguish multiple emission lines from plasma and impurities and complements the portfolio of existing Optical Emission Spectroscopy techniques, providing a good compromise regarding spectral, spatial, and temporal resolution.

© 2023 Author(s). All article content, except where otherwise noted, is licensed under a Creative Commons Attribution (CC BY) license (<http://creativecommons.org/licenses/by/4.0/>). <https://doi.org/10.1063/5.0155722>

I. INTRODUCTION

Optical Emission Spectroscopy (OES) is an established and powerful diagnostic technique for low temperature plasma characterization as present in the edge and divertor of fusion plasmas. OES is thereby a passive, non-perturbative technique with direct access to the plasma species as well as impurities that originate, e.g., from plasma-wall interaction processes. The two most common

OES methods are (i) spectrometers coupled with optical fibers to achieve the plasma emission spectrum at one specific location and (ii) CCD cameras equipped with narrow bandpass filters to get two-dimensional (2D) profiles of one specific plasma emission line. However, both methods have limitations in achieving spatial and spectral information simultaneously. Relatively, the hyperspectral imaging technique, which uses an imaging spectrometer with scanner, can simultaneously record 2D images of hundreds of narrow wavelength

spans. Compared with the two methods mentioned above, it can acquire at once spectra of more spatial locations and 2D images of more wavelength spans without any usage of fibers and narrow-band interference filters. The price to pay for this compromise is the lower spectral resolution in comparison with the state-of-the-art spectrometers and the lower spatial and temporal resolution than the state-of-the-art interference filtered CCD or CMOS cameras. Thus, the technique offers a new possibility to distinguish multiple emission lines from plasma, which also complements the portfolio of existing OES techniques, providing a good compromise regarding spectral, spatial, and temporal resolution at a moderate cost.

In this paper, a transportable hyperspectral camera (HSC) is characterized for application in steady-state plasma-material interaction experiments performed on the PSI-2 linear plasma device with tungsten (W) as the target material. First, the technical features and plasma conditions are introduced. In the following, two major applications are shown, including the measurement and imaging of T_e and n_e radial profiles as well as the application of the system in plasma-material interaction (PMI) studies aiming the W sputtering process characterization as the benchmark for PMI modeling. These applications can be improved to more advanced measurement, which also show the potentiality to transfer to fusion devices, such as tokamak and stellarator.

II. EXPERIMENTAL SETUP

Experimental data were collected at the PSI-2 linear plasma device.¹ Pure helium (He) and neon (Ne) plasma at different conditions [electron temperature (T_e) ~ 0.8 – 13.4 eV and electron density (n_e) $\sim 0.2 \times 10^{18}$ – 3.9×10^{18} m⁻³] were generated with or without a specific target at the downstream side of the plasma column with a typical diameter of about 70 mm in a hollow profile. T_e and n_e of plasma were measured by a movable Langmuir double probe (LP), which is located ~ 365 mm away from the camera in the axial direction z . Additionally, the high-resolution spectrum of plasma with a

wide wavelength span is simultaneously obtained at the same position of LP. It is based on the measurement of a cross-dispersion spectrometer (Spectrelle) with an almost constant resolving power of more than $R = \lambda/\Delta\lambda \geq 20\,000$ over the full covered spectral range of 364–715 nm.² However, radial profiles of the plasma are usually considered to be unchanged in such distance. The maximum value of T_e and n_e as well as ion flux is usually located at 2–2.5 cm from the plasma center in the radial direction, so samples are usually located at $r = 2.5$ cm.

The target can be biased for the purpose of PMI experiments with focus on physical sputtering up to -100 V, and the plasma space potential was measured to be ~ -20 V. The surface temperatures at the target material were measured using a thermocouple, pressed on the backside of the target with samples of the dimension of 1×1 cm².

The HSC was installed in front of port 3.1 [about 60 cm between the camera lens (focal length: 21 mm) and plasma center], as shown in Fig. 1. The region of interest (ROI) of the camera is ~ 170 mm in axial direction z . Figure 2(a) shows the typical field of view (FoV) of the HSC in PSI-2. In this paper, the cylindrical coordinate was used, which is z for the axial direction and r for the radial direction ($r = 0$, $z = 0$ was fixed to the center of the target surface).

III. HSC AND DATA ANALYSIS

The most common commercial HSCs are of push-broom line scanning type, which mainly consist of a front lens, an imaging spectrograph, and a detector. As the light traverses through the objective lenses, it is constrained by an entrance slit ($42 \mu\text{m} \times 11.7$ mm for Specim IQ), which serves as a spatial filter. The slit functions to limit the width of the light, allowing only a narrow portion of the object or scene to pass through. Subsequently, the light goes through the collimating optics, and the dispersing element (typically a diffraction grating) on the sensor (CMOS, CCD, sCMOS, etc.)^{3–5} disperses the light into different wavelengths, forming the “spectral” axis. By combining the spatial information obtained from the slit, both spatial

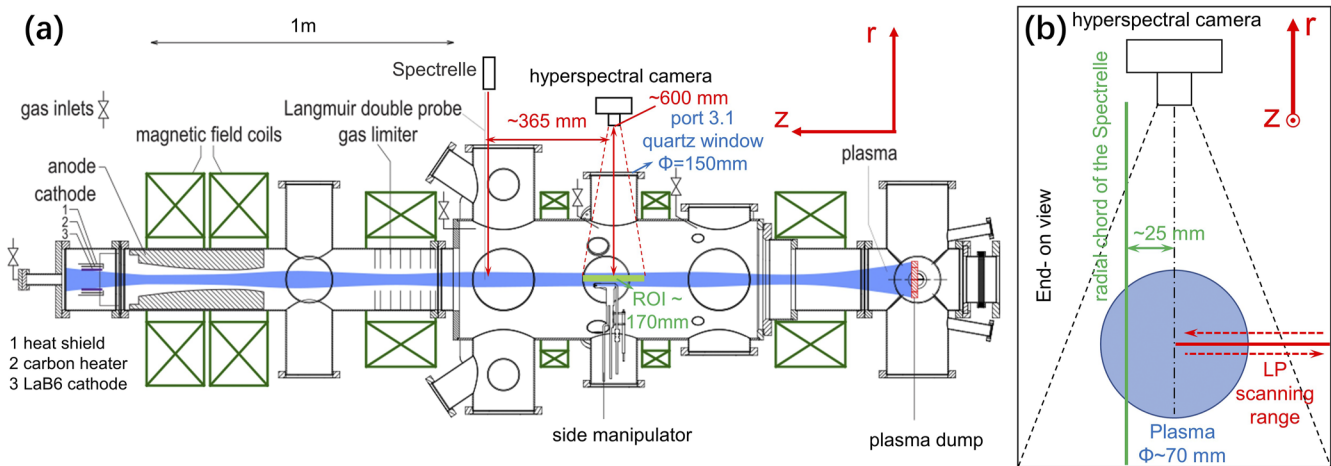


FIG. 1. (a) PSI-2 layout as well as HSC, LP, and Spectrelle setup (top view). (b) The spatial range of HSC, the LP scanning range, and the radial chord of the Spectrelle (end-on view).

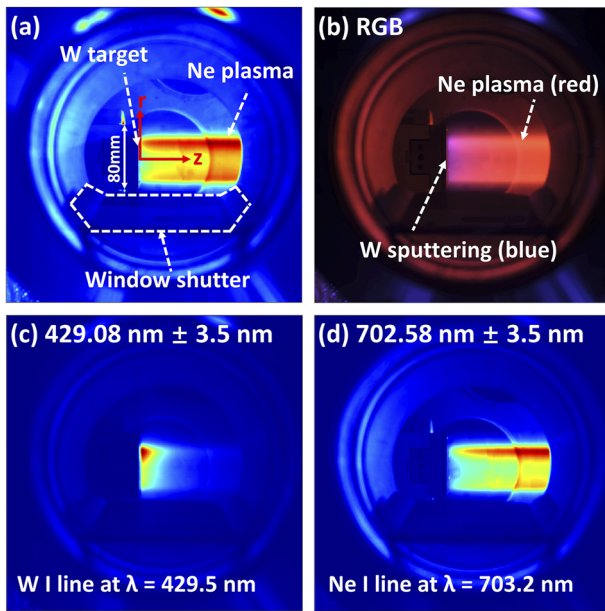


FIG. 2. An example measured by the HSC: a W target sputtered by a Ne plasma under perpendicular impact in PSI-2: (a) false color image of average intensity; (b) true color image transferred by hyperspectral data; and false color image at camera spectral bands of (c) at 429.08 nm for W I and (d) 702.58 nm for Ne I.

and spectral data of a single line (x, λ) are recorded. Through spatial scanning by an internal or external scanner, the HSC is capable of generating a data cube (x, y, λ).

A. Technical features

The HSC Specim IQ uses a CMOS sensor (type: push broom, dynamic range: 12-bits, size: $207 \times 91 \times 74 \text{ mm}^3$) in the spectral range of 400–1000 nm, and it was applied to the linear plasma device PSI-2 from a side view port of $d = 600 \text{ mm}$. The main technical specifications of Specim IQ are listed in Table I. The HSC can image the plasma in 2D—here r and z direction—with an array of $512 \times 512 \text{ pixels}^2$ at 204 different wavelength spans (an interval central wavelength of 2.88–3.09 nm and mean FWHM $\sim 7 \text{ nm}$). An example of the He plasma emission spectrum is presented in Fig. 3, which shows that the spectral resolution is sufficient to resolve major emission lines in low ionizing PSI-2 plasma at a moderate magnetic field of 0.08 T. Two He I lines at 501.6 and 504.8 nm will be treated as one line for further analyses as they cannot be resolved with the spectral resolution of 7 nm of the present system (FWHM, full width at half maximum). The exposure time is 1–500 ms/full spectrum of one line (512 pixels), and it requires 30–286 s for recording one full 2D image (512 lines). The spatial resolution can be calculated by the following formula:

$$R_s = 2 D \tan(\theta/2) / n, \quad (1)$$

where R_s (mm/pixel) is the spatial resolution, D (mm) is the distance between the object and camera, θ is the angle of field of view, and n is the spatial sampling, which is 512 for Specim IQ. Finally, R_s of

TABLE I. Main technical specification of Specim IQ.

Feature	Value
Wavelength range (nm)	400–1000
F/number	F/1.7
Spectral resolution (FWHM, nm)	7
Sensor	CMOS
Spatial sampling (pixels)	512
Spectral bands	204
Dynamic range (bit)	12
Working distance (mm)	150– ∞
Focal length (mm)	21
Full field of view (deg)	31×31

$\sim 0.6 \text{ mm/pixel}$ was acquired at a distance of $\sim 0.6 \text{ m}$ from the PSI-2 plasma with a typical FoV of $33 \times 33 \text{ cm}^2$ in this setup.

B. Data acquisition and processing

The Specim IQ records four different data cubes (three-dimensional data array, x, y, λ) of digital number (DN), which are raw data, dark frame, white reference, and processed reflectance data. The raw data (I_{raw} , DN band $^{-1}$) and dark frame (I_{dark} , DN band $^{-1}$) data cubes are used for our further analysis, while the reflectance data cube is used for other usage. It is noted that the dark frame is the baseline signal due to the camera electronics, which changes with the temperature of the sensor and integration time. I_{dark} are simultaneously recorded during the data acquisition, and it should be subtracted during data processing. First, the raw intensity counts I_{count} (DN s $^{-1}$ band $^{-1}$) are achieved as follows:

$$I_{\text{count}} = (I_{\text{raw}} - I_{\text{dark}}) / t_{\text{int}}, \quad (2)$$

where t_{int} (s) is integration time. Then, spectral sensitivity [S, (W s DN $^{-1}$ m $^{-2}$ sr $^{-1}$ nm $^{-1}$) $^{-1}$] of Specim IQ and transmissivity (τ) of the viewing window are calibrated with an integration sphere standard light source (Labsphere, USS-600). The resulting calibrated

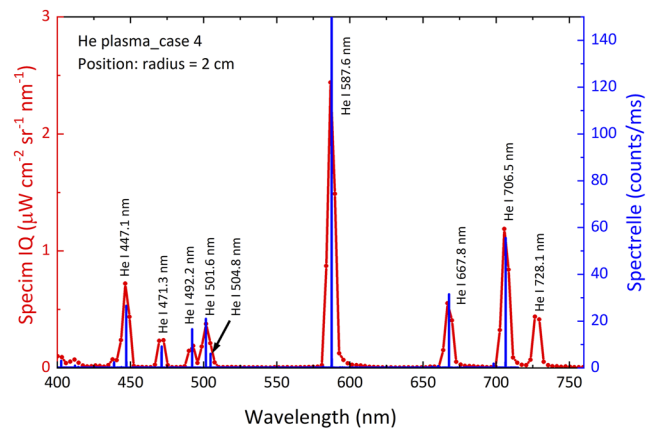


FIG. 3. Comparison of He plasma emission spectrum measured by Specim IQ (red) and Spectrelle (blue) at $r = 2 \text{ cm}$ (case 4 in Table III).

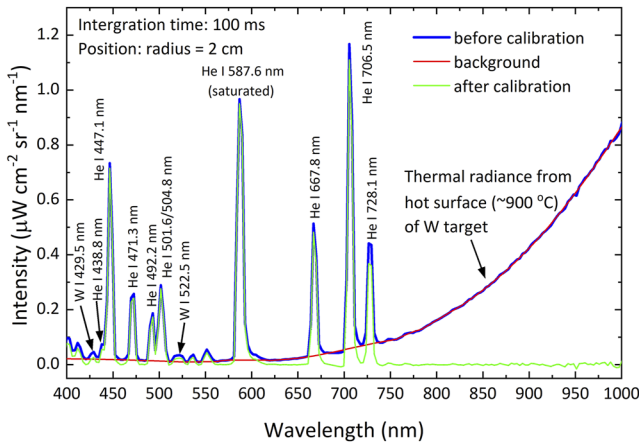


FIG. 4. An example to remove the background of thermal radiance in the spectrum taken by hyperspectral. The spectrum is taken 5 mm in front of a W target in He plasma, which is -100 V biased with ~ 900 °C surface temperature.

intensity (I_{cal} , $\text{W m}^{-2} \text{sr}^{-1} \text{nm}^{-1}$) can be calculated by the following equation:

$$I_{cal} = I_{count} / (S \cdot \tau). \quad (3)$$

It should be noted that I_{raw} , I_{dark} , I_{count} , and I_{cal} are the matrices with the dimension of $512 \times 512 \times 204$ (x , y , λ), which refer to the spatial (x , y) and spectral (λ) information, respectively.

C. Background/continuum emission subtraction

The background emission, which results from stray light (impurities radiation, molecular spectrum, bremsstrahlung, etc.) and thermal radiation from the hot surface at the target, should also be subtracted before the detailed analysis of hyperspectral imaging data. The background signal (I_{BG}) is subtracted from calibrated intensity (I_{cal}), and the averaged total intensity (\bar{I}_{tot}) at a specific wavelength λ with typical full width at half maximum (FWHM, 7 nm for Specim IQ) can be obtained as

$$\bar{I}_{tot}(\lambda) = I_{cal}(\lambda) - I_{BG}(\lambda). \quad (4)$$

Since the whole spectrum is obtained at once, I_{BG} can be easily estimated by the neighboring wavelength bands of the intended emission line.⁶ An example to remove the background signal of thermal radiation is presented in Fig. 4. The measurement is taken in He plasma, which is located ~ 2.5 mm in front of a heated W target with a temperature of ~ 900 °C. Thermal radiation from the target is reflected by the inner wall of the chamber and in this case superposed with the He and W emission lines to be analyzed.

IV. APPLICATION

As the HSC acquires a data cube, multiple functions can be obtained. For example, the HSC can get similar results as CCD, color, and filtered cameras with the same FoV, as depicted in Fig. 2. As the spectra with acceptable spectral resolution are recorded at the same time, thermal backgrounds and changes in, e.g., emissivity can be taken into account in the further spectral analysis possible.

A. Measurement and imaging of T_e and n_e profiles

As studied before in fusion plasma application, He I line ratios, especially 667.8/728.1 and 728.1/706.5 nm, are sensitive to and usually used to measure n_e and T_e of divertor and scrape-off layer plasmas, respectively.⁷ By comparison of measured line intensity ratios with those obtained by a collisional-radiative model (CRM), the profiles of T_e and n_e can be evaluated until He is ionized in a tokamak plasma.⁸ However, due to the limitation of spectral resolution, the direct use of CRM needs more data processing and calibration. According to Ref. 9, a simple statistical approach, comparable to machine learning methodology, was adopted, which acquire T_e and n_e profiles via calibration of multiple He line ratios with LP measurements at the linear plasma device for a dataset of different plasmas.⁹ Note that line-integrated vertical profiles of intensity can be directly treated as radial profiles without Abel inversion in such a approach.⁹

The scaling law for prediction of n_e and T_e from He I line ratios was examined. Six line ratios made of seven strong low level He I lines from 400 to 800 nm (except the He I line at 587.6 and 402.6 nm) in Fig. 3 were considered. The optical transitions of neutral He in the HSC spectral range are listed in Table II,¹⁰ and a power function is assumed from each line ratios as follows:

$$T_e \text{ or } n_e = \alpha \cdot r_0^{c_0} \cdot r_1^{c_1} \cdot r_2^{c_2} \cdot r_3^{c_3} \cdot r_4^{c_4} \cdot r_5^{c_5}, \quad (5)$$

where α and c_0 , c_1 , c_2 , etc., are fitting parameters. r_n ($n = 1, 2, 3, \dots$) are the intensity (I) ratios between two He lines, $r_0 = I_{667.8}/I_{728.1}$, $r_1 = I_{706.5}/I_{728.1}$, $r_2 = I_{501.6/504.8}/I_{728.1}$, $r_3 = I_{492.2}/I_{728.1}$, $r_4 = I_{492.2}/I_{471.3}$, and $r_5 = I_{492.2}/I_{447.1}$. The subscript of I is the wavelength (nm) of the specific He I line. Then, these fitting parameters can be obtained by multiple linear regression fit, T_e and n_e are

TABLE II. Optical transitions of He I in the HSC spectral range between 400 and 1000 nm.

Wavelength (nm)	Species	Transition
447.1	Triplet	$4^3D \rightarrow 2^3P$
471.3	Triplet	$4^3S \rightarrow 2^3P$
492.2	Singlet	$4^1D \rightarrow 2^1P$
501.6	Singlet	$3^1P \rightarrow 2^1S$
504.8	Singlet	$4^1S \rightarrow 2^1P$
587.6	Triplet	$3^3D \rightarrow 2^3P$
667.8	Singlet	$3^1D \rightarrow 2^1P$
706.5	Triplet	$3^3S \rightarrow 2^3P$
728.1	Singlet	$3^1S \rightarrow 2^1P$

TABLE III. Range of probe-measured n_e and T_e in PSI-2 at different He plasma conditions.

	P_{He} (mbar)	T_e (eV)	n_e (10^{18} m^{-3})
Case 1	5.5×10^{-5}	2.5–9.1	0.9–3.1
Case 2	1.4×10^{-5}	1.0–6.5	0.5–3.9
Case 3	1.4×10^{-5}	0.8–4.7	0.3–2.5
Case 4	...	3.9–13.4	0.2–0.8

taken from the Langmuir probe, and r_n are taken from the HSC. There are three cases of plasma (cases 1–3) with different conditions (154 data points) in Table III for the calculation of regression or, in modern other words, AI training and one case (case 4) for comparison of LP measure and calculation of line ratios. In Fig. 5, fitted T_e and n_e results are compared with probe-measured data, which show the error generally within $\pm 20\%$ (red line). The acceptable error makes it possible to measure plasma parameters by HSC. Figure 6 shows the comparison of T_e and n_e radial profiles in He plasma of cases 1–4, which are measured by LP (lines) and calculated by line ratios (scatter), while Fig. 6(a) is for regression and Fig. 6(b) is for comparison. Figure 7 shows the 2D distribution of calculated T_e and n_e of He plasma based on camera measurement. The plasma parameters are deduced by the spectrum of every specific pixel, which are based on Eq. (5) with calibrated fitting parameters. Although the linear plasma parameters are usually treated to be symmetric in the radial direction and are unchanged along the axial direction, the 2D images of T_e and n_e are still slightly asymmetric and change in both directions. This shows the sensitivity of HSC, which would be potentially suitable for the application of precision

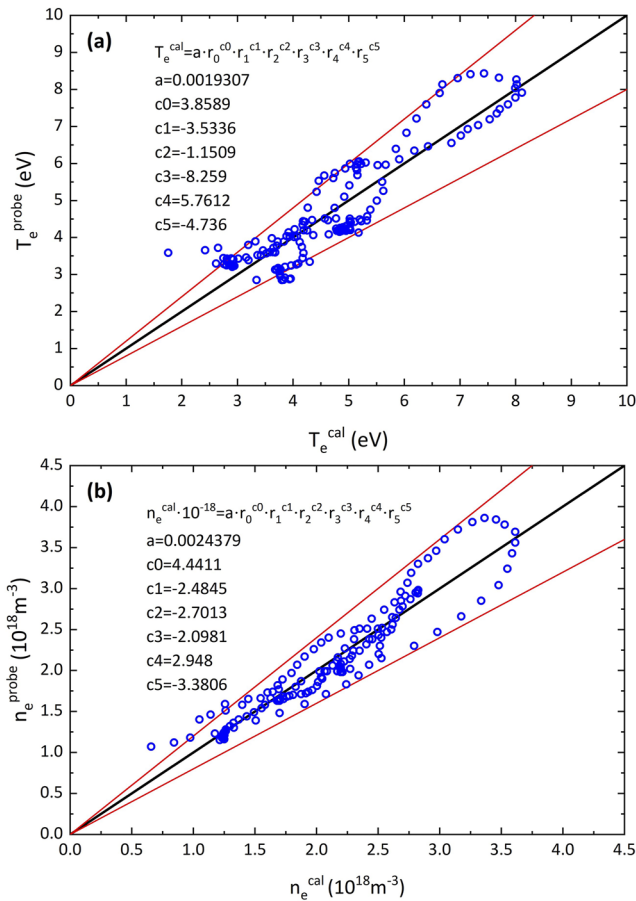


FIG. 5. Comparison of (a) T_e and (b) n_e measured by LP and calculated using line ratios [Eq. (5)]. The superscripts “probe” and “cal” indicate LP measurements and line ratio calculations, respectively.

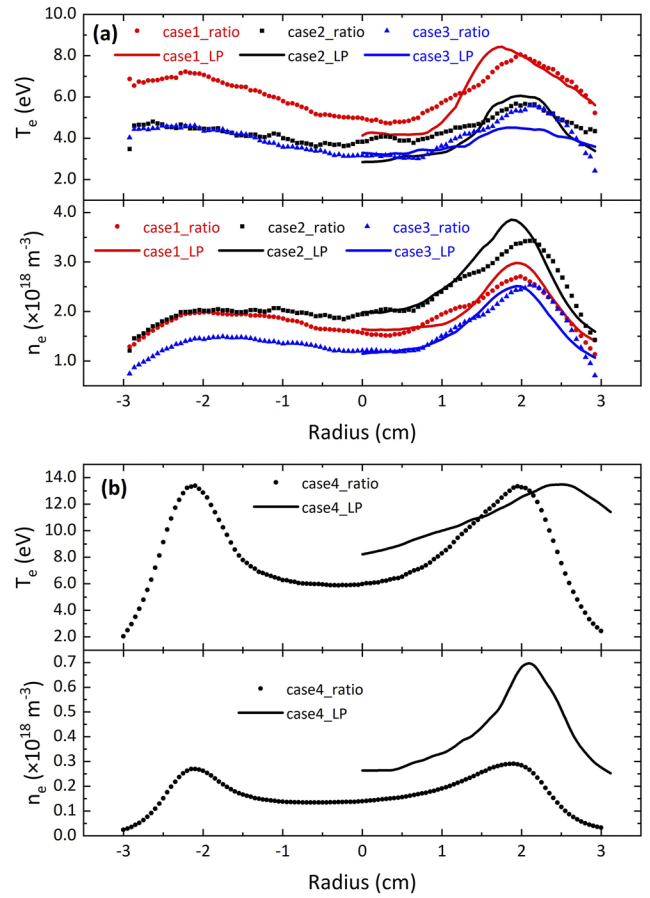


FIG. 6. Comparison of T_e and n_e radial profiles in He plasma, which are measured by LP (lines) and calculated by line ratios (scatter). (a) Cases 1–3 are data for regression and (b) case 4 is data for comparison.

measurement. What is more, it can be foreseen that it would be interesting to apply in plasma with sputtered impurities, whose T_e and n_e would be different near the target.

This is regarded as one of the most remarkable applications of HSC for plasma diagnostics, i.e., to replace moderately perturbing LP without interfering with plasma conditions. Apart from the perturbation-free measurement, the provision of 2D profiles, in this case z - and r -direction, is the most important capability and permits direct comparison with modeling predictions. Moreover, the HSC can be applied in any environment that can only be optically assessed, such as, e.g., in hot cell conditions as foreseen in the future in the PSI-2 twin JULE-PSI.¹¹

B. Application in PMI studies

The W sputtering study is also carried out as a proof-of-concept experiment for a combined plasma diagnostic and PMI study in the linear device. A negatively biased W target (-100 V) is exposed to a Ne plasma, ensuring that W can be sputtered by Ne^+ ions with known energy under controlled conditions. The red Ne plasma, dominated by multiple Ne I lines in the red spectral region, and the

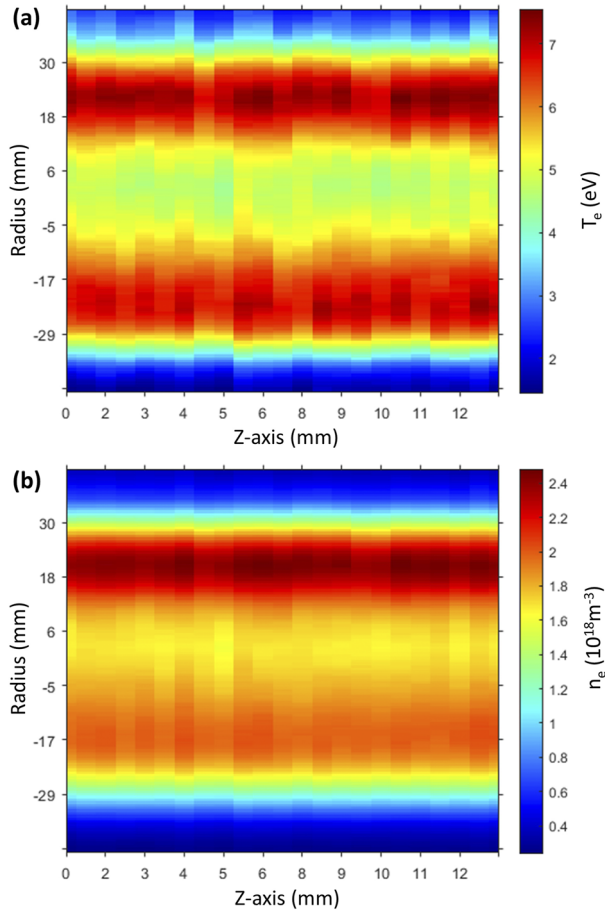


FIG. 7. 2D distribution of calculated (a) T_e and (b) n_e of He plasma based on camera measurement (case 1 in Table III, smoothed in the radial direction).

blue light from the sputtered W target, dominated by multiple W I lines in the blue spectral region, can be directly observed by the camera, as seen in Fig. 2(b). After a more detailed analysis of the emission spectrum, the signal of the sputtered W and Ne plasma background can be separated. Figure 8 shows the camera band at 429.08 nm (central wavelength, FWHM = 7 nm) dominated by the W I line signal at 429.5 nm for the W I transition $5d^5(^6S)6p^7P_2 \rightarrow 5d^5(^6S)6s^7S_3$, which can be chosen to represent the distribution of sputtered W. Thus, the HSC can clearly distinguish W impurities from Ne plasma in full 2D as imaged in Figs. 2(c) and 2(d) at one measurement without changing interference filters. This provides a big advantage for future benchmarking models, such as ERO2.0.¹²

V. SUMMARY

The HSC Specim IQ has been applied at linear plasma device PSI-2 for steady-state plasma diagnostics. Two major applications, plasma diagnostics in He plasmas and PMI studies between Ne and W, have been demonstrated, providing the measurement and 2D imaging of T_e and n_e radial profiles as well as the 2D images of the sputtered W atom emission line, respectively.

The advantages of such HSC have been mentioned in previous studies.⁶ (i) It is convenient to acquire both spectral and spatial information at once, which means without the use of filters and optical fibers that need to be included in the analysis of data. (ii) The background/continuum emission subtraction is convenient in the HSC system compared to filtered cameras. Because HSC is capable of capturing a wide spectral range, eliminating the need for multiple bandpass filters and dedicated calculations required filtered cameras or filterscope detection in tokamaks.^{13–16} (iii) A good overview spectrum in a large wavelength range is obtained. However, drawbacks exist and need to be considered in the planning of experiments: (i) Features of line-scanning may not be suitable for non-stationary plasmas even when slow transient events in plasma

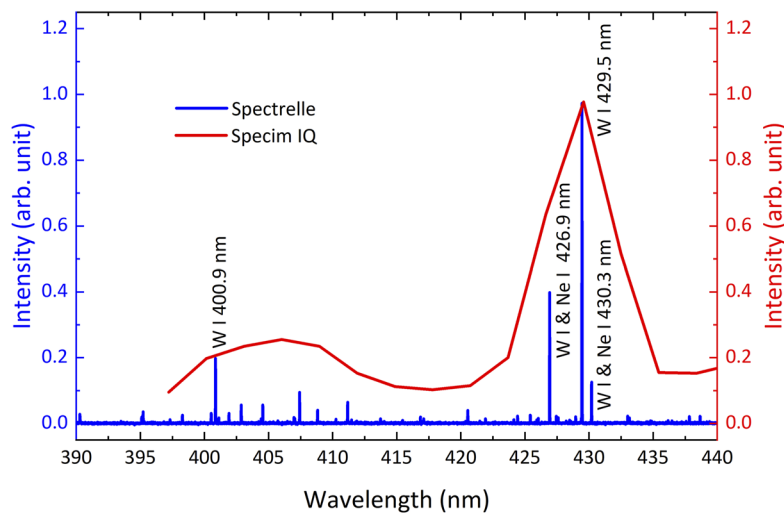


FIG. 8. Comparison of spectra obtained by Spectrelle (blue curve) and Specim IQ (red curve). The spectrum was captured ~5 mm from the W target in Ne plasma.

can perturb the measurement. There are novel HSCs appearing utilizing snapshot techniques, which permit 2D imaging for transient phenomena, such as ELMs in tokamaks. (ii) The spectral resolution of the present system is moderate (FWHM = 7 nm), and a resolution in the order of 1–2 nm would be advisable for comparisons with the state-of-the-art imaging techniques with single cameras and interference filters, such as in JET.¹⁷

However, combining high resolution spectrometers for spectral data validation and careful selection of the emission line can help to overcome these drawbacks and make the system also suitable for more challenging conditions as in the steady-state linear plasmas device PSI-2. Thus, with the few limitations in the use of the here presented Specim IQ in plasma and nuclear fusion research, the technique is expected to be a good new option as a diagnostic tool in steady-state plasma experiments.

Furthermore, 2D profiles of T_e and n_e will be evaluated from the He I line intensity ratios and will be then used as an input to the impurity transport simulation codes. In addition to plasma observations, Specim IQ can be applied to the characterization of plasma-exposed surfaces: the relationship between reflectance, emissivity, surface morphology, etc.

ACKNOWLEDGMENTS

This work was subsidized by the National Key R&D Program of China under Contract No. 2022YFE03030000. This work was carried out within the framework of the EUROfusion Consortium, funded by the European Union via the Euratom Research and Training Program (Grant Agreement No 101052200—EUROfusion), was subsidized by the Key Research Program of Frontier Sciences of CAS with Grant No. ZDBS-LY-SLH010 and the programs of the National Natural Science Foundation of China (Grant Nos. 12205332, 12205333, 12022511, and 12261131496) and was supported by the 2020 Helmholtz-OCPC Fellowship Program. Views and opinions expressed are, however, those of the author(s) only and do not necessarily reflect those of the European Union or the European Commission. Neither the European Union nor the European Commission can be held responsible for them.

AUTHOR DECLARATIONS

Conflict of Interest

The authors have no conflicts to disclose.

Author Contributions

Changjun Li: Conceptualization (equal); Data curation (equal); Methodology (equal); Validation (equal); Writing – original draft (equal). **Sebastijan Brezinsek:** Conceptualization (equal); Data curation (equal); Project administration (equal); Resources (equal); Supervision (equal); Writing – review & editing (equal). **Stephan Ertmer:** Data curation (equal); Writing – review & editing (equal). **Arkadi Kreter:** Data curation (equal); Writing – review & editing (equal). **Michael Reinhart:** Data curation (equal); Writing – review & editing (equal). **Rui Ding:** Data curation (equal); Resources (equal); Supervision (equal); Writing – review & editing (equal). **Junling Chen:** Resources (equal); Supervision (equal); Writing – review & editing (equal).

DATA AVAILABILITY

The data that support the findings of this study are available from the corresponding author upon reasonable request.

REFERENCES

- ¹ A. Kreter, C. Brandt, A. Huber *et al.*, *Fusion Sci. Technol.* **68**, 8–14 (2017).
- ² S. Brezinsek, M. Laengner, J. W. Coenen *et al.*, *Phys. Scr.* **T170**, 014052 (2017).
- ³ P. Mishra, M. S. M. Asaari, A. Herrero-Langreo *et al.*, *Biosyst. Eng.* **164**, 49–67 (2017).
- ⁴ M. Piccolo, C. Cucci, A. Casini *et al.*, *Sensors* **20**, 2843 (2020).
- ⁵ J. Behmann, K. Acebron, D. Emin *et al.*, *Sensors* **18**, 441 (2018).
- ⁶ D. Nishijima, M. I. Patino, and R. P. Doerner, *Rev. Sci. Instrum.* **91**, 083501 (2020).
- ⁷ B. Schweer, M. Brix, and M. Lehnen, *J. Nucl. Mater.* **266–269**, 673–678 (1999).
- ⁸ O. Schmitz, I. L. Beigman, L. A. Vainshtein *et al.*, *Plasma Phys. Control. Fusion* **50**, 115004 (2008).
- ⁹ D. Nishijima, S. Kajita, and G. R. Tynan, *Rev. Sci. Instrum.* **92**, 023505 (2021).
- ¹⁰ A. Kramida, Y. Ralchenko, J. Reader, *et al.* (2022)., NIST Atomic Spectra Database, version 5.10, <https://physics.nist.gov/asd>, 2022.
- ¹¹ B. Unterberg, R. Jaspers, R. Koch *et al.*, *Fusion Eng. Des.* **86**, 1797–1800 (2011).
- ¹² A. Eksaeva, D. Borodin, J. Romazanov *et al.*, *Phys. Scr.* **T171**, 014057 (2020).
- ¹³ T. Abrams, D. M. Thomas, E. A. Unterberg *et al.*, *IEEE Trans. Plasma Sci.* **46**, 1298–1305 (2018).
- ¹⁴ O. Meyer, J. C. Giacalone, A. Gouin *et al.*, *Rev. Sci. Instrum.* **89**, 10D105 (2018).
- ¹⁵ A. Huber, S. Brezinsek, A. Kirschner *et al.*, *Nucl. Mater. Energy* **18**, 118–124 (2019).
- ¹⁶ A. N. James, D. Brunner, B. Labombard *et al.*, *Plasma Phys. Control. Fusion* **55**, 125010 (2013).
- ¹⁷ J. Karhunen, A. Holm, B. Lomanowski *et al.*, *Plasma Phys. Control. Fusion* **64**, 075001 (2022).